ADVANCED OPTICAL MATERIALS
www.advopticalmat.de

Few Photons Probe Third-Order Nonlinear Properties of Nanomaterials in a Plasmonic Nanocavity

*Anupa Kumari, MohammadReza Aghdaee, Mathis Van de Voorde, and Oluwafemi Stephen Ojambati**

Quantification of nonlinear optical properties is important for nano-optical devices, yet such measurements remain challenging at the single-particle level. Here, enhanced optical fields are harnessed inside a plasmonic nanocavity to mediate efficient nonlinear interactions with an individual particle. Reflection Z-scan technique was performed on individual nanocavities, reaching down to two photons per pulse, thus demonstrating a significantly higher efficiency beyond conventional methods. The few photons are sufficient to extract the nonlinear refractive index and nonlinear absorption coefficient of different nanomaterials, including perovskite and Au nano-objects and a molecular monolayer. This work is of great interest for investigating nonlinear optical interactions on the nanoscale and characterizing nanomaterials, including fragile biomolecules.

1. Introduction

Nonlinear optical materials are essential in advanced photonics, serving as building blocks for devices such as optical limiters, saturable absorbers, and optical switches.[1–3] Moreover, on the nanoscale, there is also a growing demand for the exploitation of nonlinear optical devices in photonic circuits and chips.[4,5] An accurate determination of the nonlinear optical properties is, therefore, valuable. Particularly, these applications require a quantification of nonlinear susceptibilities $\chi^{(N)}$, $N = 3, 5, \ldots$, with real and imaginary parts related to the nonlinear refractive index and nonlinear absorption coefficient, respectively.

A. Kumari, M. Aghdaee, M. Van de Voorde, O. S. Ojambati
Faculty of Science and Technology
MESA+ Institute
University of Twente
Enschede 7522NB, the Netherlands
E-mail: o.s.ojambati@utwente.nl

M. Van de Voorde
Institute of Microstructure Technology
Karlsruhe Institute of Technology
76131 Karlsruhe, Germany

The ORCID identification number(s) for the author(s) of this article can be found under https://doi.org/10.1002/adom.202403484

DOI: 10.1002/adom.202403484

However, there is still a knowledge gap in determining the nonlinear optical properties from a single nanomaterial.[6,7] This knowledge gap is due to the absence of a straightforward experimental method that efficiently focuses optical fields on the nanomaterial. There are various demonstrations of nonlinear optical effects on nanomaterials including four-wave mixing, high harmonic generation, two-photon absorption, optical Kerr effect, nonlinear spectroscopy and supercontinuum generation.[7–12] Despite the popularity of these observations, nonlinear optical properties are often inferred indirectly, making data interpretation complex and less straight forward.[13]

Z-scan method is a popular experimental technique to directly determine the third-order nonlinear refractive index (n_2) and nonlinear absorption coefficient (β) of various materials.[14,15] In the Z-scan experiment, as a sample translates through an optical focus, changes in transmitted or reflected intensities are compared with a theoretical model. The fitting parameters of the model are n_2 and β. The Z-scan technique has two main limitations: First, it is not yet suitable for characterizing single-particle nanomaterials because the incident field is focused on an area of about tens of μm^2. Thus, the intensity is inefficiently distributed on a single nanoparticle. Second, the existing Z-scan measurements still require high intensities of the order of GW cm^{-2} (e.g. ref. [16]). Such high intensities pose a significant risk of damaging nanomaterials, particularly delicate structures like biomaterials.

Plasmonic nanostructures are a possible solution to overcome the challenges of measuring the nonlinear optical properties of individual nanomaterials. The nanostructures localize optical fields in a sub-diffraction-limited spot, due to induced collective oscillations of free electrons.[17] The localized fields can efficiently concentrate the intensity on a single nanomaterial as well as enhance nonlinear optical interactions due to substantial field enhancements.[18–23] Various configurations of metallic nanostructures have been experimentally investigated, including point-point, point-plane, and plane-plane configurations.[24] These configurations exploit the strong near-field interactions with molecules, resulting in modifications of electronic states, albeit in the linear regime. The plasmonic effect enabled earlier studies to perform Z-scan experiments at low intensities (in the range of kW cm^{-2} to MW cm^{-2}), but using a large focused laser beam on an area of 20–40 μm^2.[25,26] Therefore, the

measurements encompass multiple nanoparticles, resulting in a signal that is an ensembled response from multiple nanoparticles rather than a single nanoparticle. However, a method that efficiently harnesses the localized optical field to probe the nonlinear optical properties of individual nanomaterials is still lacking.

In this paper, we measure the third-order nonlinear optical properties, namely n_2 and β, of nanoscale materials inside a plasmonic nanocavity. The plasmonic nanocavity is made of Au nanoparticle that is separated by the material to be characterized from a Au film. Optical fields are enhanced inside the nanocavity,[27,28] thus providing a suitable environment for efficient nonlinear optical light-matter interactions. We demonstrate that the highly efficient nanocavity enables low-intensity illumination down to a few photon levels.

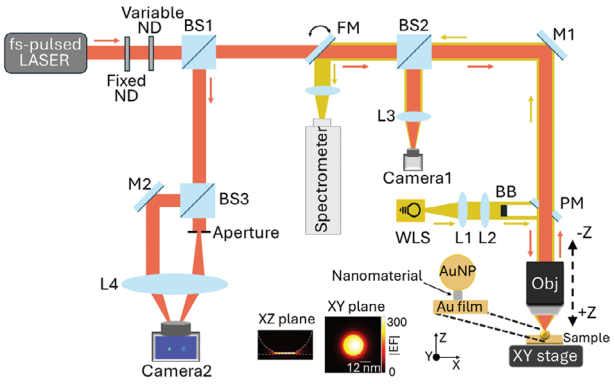

Figure 1. Schematic of reflection Z-scan experimental setup. L1, L2, L3, L4: lens; M1, M2: mirror; PM: perforated mirror; ND: neutral density filter; BS1, BS2, BS3: beam splitter; FM: flipping mirror; WLS: white light source; BB: beam blocker. Inset: Numerical calculation results of the electric field enhancement (EF) at different cross sectional planes. The dashed curves show the boundary of the nanoparticle and the Au film.

2. Experimental Section

2.1. Measurement Principle and Setup

To determine the third-order nonlinear properties, the reflection Z-scan (RZ-scan) technique was used. The measurement principle was as follows: The reflected light was measured in two configurations, open aperture (OA) and closed aperture (CA), as the sample moves through the profile of a focused laser beam. In the OA configuration, the reflected light was collected by a lens and measured by a detector. The OA configuration provides information about n_2 due to the nonlinear photo-induced modification of the reflection coefficient of the surface. Whereas for CA, only a part of the beam passing through an aperture was collected by the detector. The CA captures the nonlinear phase change of the reflected beam due to the nonlinear absorption. No nonlinear effects appear when the sample was positioned far from the focal plane, and therefore, the reflected laser beam in this region was constant. To provide insight into the beam spatial profile within the nanocavity, numerical simulations were performed using the boundary element method (BEM) for a gap size of 0.9 nm, corresponding to the thickness of the methylene blue layer. The enhanced electric field is strongly confined within the nanocavity and extends over the entire area under the nanocavity (Inset **Figure 1**).

In the experiment, a combined RZ-scan setup and a darkfield microscopy-spectroscopy setup (Figure 1) (for more details, see the Supporting Information) was employed. A femtosecond pulsed laser delivers 120 fs optical pulses with a tunable wavelength in the near-infrared region. The pulses have a repetition rate of 76 MHz and an average output power of 1 W. A combination of variable and fixed neutral density filters control the intensity that illuminates the sample. The laser pulse was focused onto the sample using a brightfield/dark-field microscope objective with a numerical aperture of 0.9. The microscope objective translates in the Z-direction, bringing the sample through the optical focus. The sample was mounted on an XY translation stage to measure multiple nanocavities. The darkfield microscopy-spectroscopy setup images the nanoparticles on the Au film and measures their extinction spectra to reveal the resonance of the individual plasmonic cavity.

2.2. Sample

Three nanomaterials were investigated inside the plasmonic nanocavity: 1) a 10 nm Au nano-object, 2) a 6.5 nm Yb^{3+}:$CsPbCl_3$ perovskite nano-object, and 3) a monolayer of methylene blue molecule, that is 0.9-nm thick. (For details about the sample fabrication and characterization, see Supporting Information). The samples enable a comparison of the nonlinear effects inside the nanocavity at different gap sizes and nonlinear optical properties. The samples were chosen as a proof of concept to demonstrate the versatility of the technique that was applicable to different types of nanoparticles or molecular layers. These nanomaterials have significant applications in various nonlinear optical fields. Methylene blue, a fluorescent dye, is widely used in biomedical imaging and therapy, particularly in multiphoton excitation fluorescence microscopy, and as a saturable absorber in ultrafast laser systems. Gold nanoparticles have applications that range from bioimaging and sensors and optical limiting to optical switches in integrated photonics. In addition, perovskites are well-known for their exceptional optoelectronic properties, making them highly valuable in the application of solar cells. A bare Au film without a nanomaterial serves as a reference sample. For all the samples, an atomically flat Au film was used with a thickness of 40 nm instead of a thicker film (⩾100 nm). The thin Au film allows for a considerable scattered intensity from the nanocavity and reduces reflection from the Au film (For experimental data, see Figure S1, Supporting Information). Gold nanoparticles (80 nm diameter) were drop-casted on the materials on the Au film to form the nanocavity.

3. Results and Discussion

We probe the Au nano-objects in the nanocavity at two laser powers of 48 pW and 700 pW, corresponding to 2 and 34 photons per pulse on average, respectively, at 750 nm. The OA Z-scan trace shows that the reflectance peaks around the focus (**Figure 2a**). On the other hand, the CA Z-scan trace shows a peak-to-valley signature, meaning that the reflectance increases in the prefocal

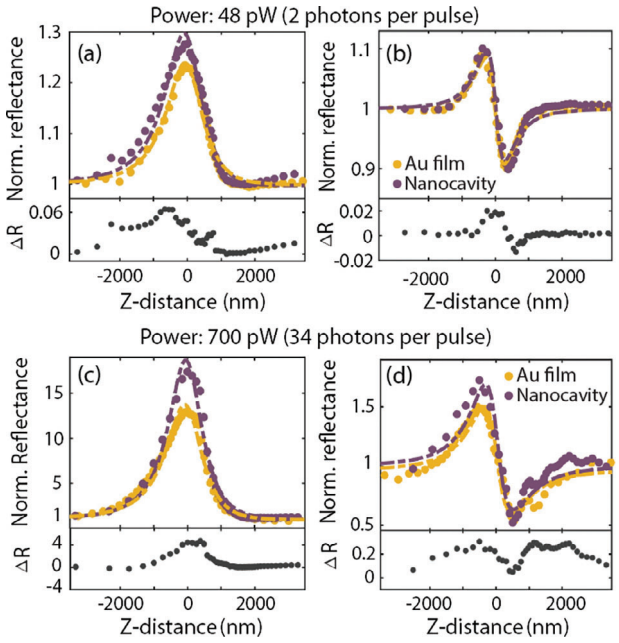

Figure 2. Normalized reflectances *vs* Z-distance for open a,c) and closed aperture b,d) measurements on the nanocavity (purple) and on the gold film (yellow) at 48 pW and 700 pW. The dotted lines represent the theoretical fit. Insets: Differential reflectance obtained by subtracting the reflectance from the Au film from that of the nanocavity.

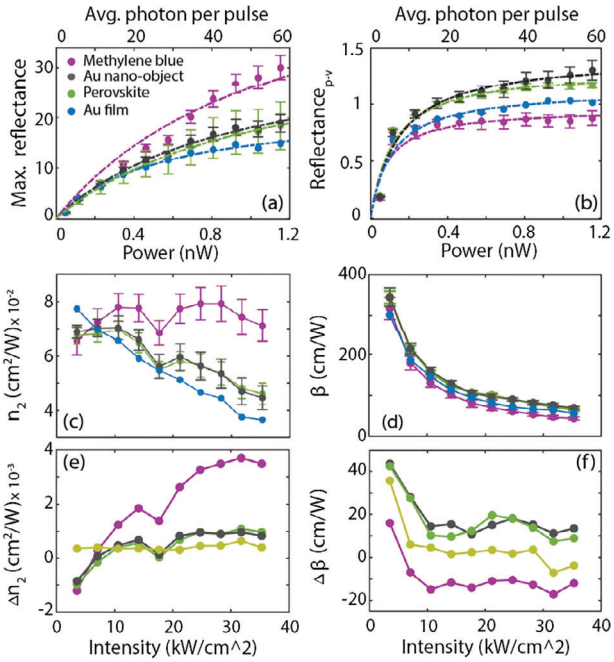

Figure 3. a,b) Maximum reflectance and the peak-to-valley (P2V) reflectance *vs* average pulse power, extracted from the open aperture and closed aperture measurements. The dotted line represents the intensity saturation fitting curve c,d) Extracted nonlinear refractive index n_2 and the nonlinear absorption coefficient β vs intensity. e,f) Nonlinear refractive index difference (Δn_2) and nonlinear absorption coefficient difference ($\Delta\beta$) between the nanocavity and the Au film. The error bar is the standard deviation of the distribution for an average of 25 nanocavities per sample.

region and decreases in the postfocal region. Conventionally, the Z-scan traces are normalized to the reflected intensity at large Z-distances away from the focus, which is the linear regime.[15,29] When the sample approaches the focal plane, the laser intensity increases, and the nonlinear effects start occurring. The experimental results of both configurations agree with the expected theoretical results, as we explain below. For the OA, the reflectance peak is attributed to positive values of the nonlinear refractive index ($n_2 > 0$) due to changes in the reflection coefficient.[30] The CA Z-scan trace follows a peak-to-valley signature, indicating a positive change in the nonlinear phase that results in positive values for the absorption coefficient ($\beta > 0$).

An interesting point to note here is the possibility of performing these measurements at extremely low photon count levels, down to an average of 2 photons per pulse. This result highlights the sensitivity of our experimental set-up to the optical excitation, which is $\approx 10^6$ more efficient than typical Z-scan techniques that use the intensity of the order of GW cm^{-2}.[31,32] Compared to the reflection from a bare Au film, there is an observable difference in reflectivity from the nanocavity. We quantify this contribution by the difference in the reflectance (ΔR) between gold film and nanocavity (insets in Figure 2). The significance of ΔR is that it is relatively low at the two-photon level but non-zero, and it becomes more pronounced at higher power (34 photons). This result thus demonstrates the efficiency of the nanocavity at these ranges of number of photons. Both the OA and CA measurements show that ΔR increases by almost 10 times between the two powers.

We performed power-dependent RZ-scan measurement on 25 nanocavities, on average, for the three different samples. We extract the maximum reflectance and the peak-to-valley reflectance from the Z-scan traces. Generally, for both OA and CA, the maximum reflectance and the peak-to-valley reflectance increase with the average pulse power (**Figure 3**a,b). In addition, both measurements show saturation behaviors, albeit at different saturation powers of 1 nW and 0.1 nW on average for OA and CA, respectively. For the OA measurements, the methylene blue layer has the highest reflectance than the Au and perovskite nano-objects, and implying that there is a higher n_2. On the other hand, the peak-to-valley reflectance of the methylene blue layer is the lowest in CA. As CA is attributed to the nonlinear absorption happening in the material, one can say that the Au and perovskite nano-objects result in a higher nonlinear absorption than when the methylene blue layer is inside the gap. In CA, the reflectance values are generally lower than OA measurements because only a part of the beam (20%) passes through the aperture.

For the quantitative estimation of the n_2, we fit the OA Z-scan traces with a theoretical model[33,34] that describes the normalized reflectance R (see Supporting Information)

$$R(x) = 1 + \frac{r\, I_0\, n_2}{(x^2+1)(x^2+9)} + \mathcal{O}(k_2') \tag{1}$$

r is the relative change in the reflection coefficient due to the nonlinear optical effects, I_0 is the laser intensity on the sample and $x = z/z_0$, z_0 is the Rayleigh length. A higher-order correction term is included as $\mathcal{O}(k_2')$, where k_2' is a small factor that accounts for

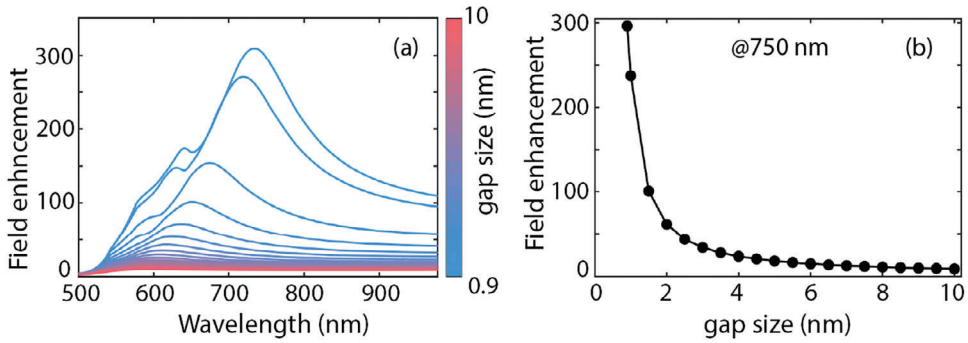

Figure 4. a) Electric field resonance as a function of wavelength and gap size. The field resonance occurs at a specific wavelength and the resonance wavelength shifts to lower wavelength as the gap size increases. b) Simulation results of electric field enhancement inside the nanocavity as a function of gap size at incident wavelength of 750 nm.

nonlinear absorption. Similarly, we model the measured CA Z-scan traces with the equation

$$R(x) = 1 - \frac{4\,r\,I_0\,x\,k_2}{(x^2+1)(x^2+9)} + \frac{r^2\,{I_0}^2\,k_2^2}{(x^2+1)(x^2+9)} + \mathcal{O}(n_2') \qquad (2)$$

that also includes higher-order correction terms that include a small contribution from nonlinear refraction, accounted for by n_2'. We extract n_2 and k_2 by fitting the Equations (2) and (3) respectively to the Z-scan traces and calculate $\beta = 2\pi k_2/\lambda$, where λ is the wavelength, for all input intensities and the materials. The extracted β for the Au film is comparable to the result (2×10^{-3} cm W^{-1} at 110 MW cm^{-2}) in the literature,[35] after accounting for the differences in the intensity and sample thickness. This agreement shows the efficacy of our extraction procedure. The n_2 for Au film displays a downward linear trend with increasing intensity. The nanocavity samples show slightly oscillatory behavior with a noticeable dip $\approx$ 17kWcm^{-2}. Similar to the Au film, the nano-objects also exhibit a downward trend, suggesting an influence from the Au film.

To obtain the n_2 values specific to the materials inside the nanocavity, we calculate the differential nonlinear refractive index Δn_2 by subtracting the n_2 values of the Au film from those of the materials.[36] We also calculated the Δn_2 of empty cavities i.e. without the methylene blue in the gap, albeit the gap size remains the same due to cucurbit[7] uril spacer. The contribution of the empty cavity differs from the result of the "filled" cavity that shows an increasing trend followed by the saturation (Figure 3e). The methylene blue layer is about four times higher Δn_2 than the nano-objects. The values of the Δn_2 of the Au and perovskite nano-objects match quite well. We attribute the n_2 values to the different optical fields confined on the nanomaterials by the nanocavity. Simulation results reveal that electric field enhancement decreases significantly as the gap size varies from 0.9 nm to 10 nm (**Figure 4**). At the excitation wavelength of 750 nm, the enhancement drops from 296 at 0.9 nm (corresponding to the size of a methylene blue layer) to 13.8 at 6.5 nm (corresponding to the size of the perovskite nano-object) and further down to 9.08 at 10 nm (Au nano-object). We observe a similar trend in our measurements: the Δn_2 is higher for methylene blue and comparable

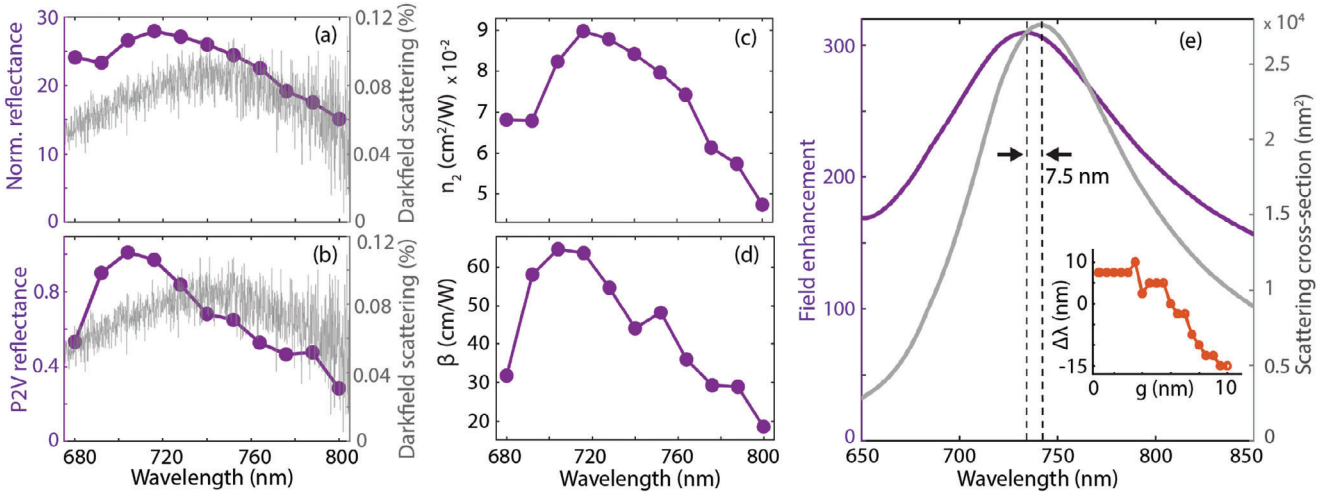

Figure 5. Excitation wavelength scan for a) OA and b) CA at an average power of 900 pW. The grey solid curve is the extinction spectrum. c,d) The extracted values of n_2 and β at different wavelengths, respectively. e) Calculated electric field enhancement and the scattering cross section as a function of wavelength (nm) for a 0.9 nm gap size. Inset: Wavelength ($\Delta\lambda$) of the maximum peak wavelengths for field enhancement and scattering cross-section as a function of gap size (g).

for nano-objects. These findings qualitatively indicate that optical fields in the gap result in different n_2 values due to modification of the reflection coefficients in the gap.

In the closed aperture measurements, β decreases with intensity for all the materials (Figure 3d). We also calculated the differential nonlinear refractive index ($\Delta\beta$) by subtracting the β values of the Au film from those of the materials along with the empty cavity. The data reveal that the methylene blue layer has negative $\Delta\beta$ values (Figure 3f), indicating saturable absorption or population inversion, which is consistent with a previous observation of lasing of methylene blue in the nanocavity.[37] In contrast, β is positive for both the nano-objects, and their values overlap at higher intensities. The positive β implies that there is nonlinear absorption (e.g. two-photon absorption), which can occur due to broad electronic states at shorter wavelengths (Figure S4, Supporting Information) for both the perovskite and Au nano-object.

Furthermore, we investigate the effect of the cavity resonance on the nonlinear interaction using the methylene blue layer in the cavity. We scanned the pulsed laser wavelength from 680 nm to 800 nm at an average power of 900 pW. Indeed, the nonlinear response of the nanocavity is dependent on wavelength, as expected (**Figure 5**). In the OA measurements, the peak response occurs ≈720 nm, while in the CA measurements, the peak is blue-shifted by ≈20 nm. The darkfield extinction spectrum has a more redshifted peak at ≈740 nm. The spectral difference is due to a phase shift of the confined field in the gap out-coupled to farfield.[38] To further investigate the spectral shift, we perform numerical simulations (in linear regime) of the wavelength dependence of field enhancement and scattering cross section for nanocavity with methylene blue in the gap. The results show that the electric field enhancement is maximum at ≈730 nm, while the scattering spectrum is at 737.5 nm (Figure 5e). This result is consistent with our observation that there is a redshift of the scattering spectrum relative to the maximum of the nonlinear parameters. However, the observed shift of 20 nm is more pronounced than the shift from the simulation of 7.5 nm. We attribute the additional spectral shift in the experiment to the phase shift due to the change in the nonlinear refractive index, i.e. (Δn_2) from the nonlinear effect that we measured. Both OA and CA experiments indicate that the nanocavity response is maximized at a specific wavelength and decreases as the wavelength moves away from this peak. These dependencies of the nonlinear parameters on wavelength show that the nanocavity resonance strongly determines the nonlinear interaction.

4. Conclusion

We use a few photons to extract the third-order nonlinear parameters (n_2 and β) of nanomaterials inside plasmonic nanocavities. The few photons are sufficient to retrieve these parameters for a single nanoparticle of different nanomaterials inside the nanocavity, namely Au and perovskite nano-objects and methylene blue monolayer. Notably, the n_2 values are much higher for a nanocavity with a high field enhancement, indicating a substantial modification of the reflection coefficient in the gap. Moreover, the β indicates two-photon absorption and saturable absorption for the nanoparticles and the molecular layer, respectively. Beyond the nanomaterials examined here, our approach is applicable to studying the nonlinear optical properties of delicate biomolecules and nanomaterials that can be easily damaged by high laser intensities. Moreover, a characterization of the nonlinear optical properties of nanomaterials can enable their applications in nonlinear optical devices such as optical switches, saturable absorbers, and optical limiters. These nonlinear effects are also exciting for quantum experiments at a few photon levels.

Supporting Information

Supporting Information is available from the Wiley Online Library or from the author.

Acknowledgements

This publication is part of the project "Three seeds for the quantum/nano-revolution" with project number NWA.1418.22.001 and the project OCENW.XS22.1.107, which are financed by the Dutch Research Council (NWO). Additionally, the Faculty of Science and Technology, University of Twente supported the project with a tenure-track start-up fund. The authors also gratefully acknowledge the financial support provided by NWO through the Knowledge and Innovation Covenant (KIC) program. This publication is part of the project Diffuse Irradiance Redirector for Efficient ConcenTration (DIRECT) (with project number KICH1.ED02.20.006 of the research programme NWO Kennis- en innovatieconvenant Innovations for Wind and Solar which is (partly) financed by the Dutch Research Council (NWO). The authors thank Klaus Boller and Herman Offerhaus for useful feedback and stimulating discussions. The authors acknowledge Damien Hudry at the Institute for Microstructure Technology at KIT for leading the synthesis efforts on the perovskite nanocrystals and Melissa Goodwin from the MESA+ institute at UT for performing STEM measurements.

Conflict of Interest

The authors declare no conflict of interest.

Data Availability Statement

The data that support the findings of this study are available from the corresponding author upon reasonable request.

Keywords

Nanoparticles, Plasmonic nanocavity, Reflection Z-scan, Third-order nonlinearity

Received: December 19, 2024
Revised: February 11, 2025
Published online:

[1] D. Dini, M. J. Calvete, M. Hanack, *Chem. Rev.* **2016**, *116*, 13043.
[2] G. Wang, A. A. Baker-Murray, W. J. Blau, *Laser Photonics Rev.* **2019**, *13*, 1800282.
[3] C. Min, P. Wang, C. Chen, Y. Deng, Y. Lu, H. Ming, T. Ning, Y. Zhou, G. Yang, *Opt. Lett.* **2008**, *33*, 869.
[4] L. Sirleto, G. C. Righini, *Micromachines* **2023**, *14*, 614.
[5] A. F. Koenderink, A. Alù, A. Polman, *Science* **2015**, *348*, 516.

[6] M. Lippitz, M. A. van Dijk, M. Orrit, *Nano Lett.* **2005**, *5*, 799.
[7] T. Schumacher, K. Kratzer, D. Molnar, M. Hentschel, H. Giessen, M. Lippitz, *Nat. Commun.* **2011**, *2*, 333.
[8] Y. Wang, C.-Y. Lin, A. Nikolaenko, V. Raghunathan, E. O. Potma, *Adv. Opt. Photon.* **2011**, *3*, 1.
[9] L. Bonacina, P.-F. Brevet, M. Finazzi, M. Celebrano, *J. Appl. Phys.* **2020**, *127*, 23.
[10] X. Lu, D. Punj, M. Orrit, *Nano Lett.* **2022**, *22*, 4215.
[11] S. Tomita, T. Kato, S. Tsunashima, S. Iwata, M. Fujii, S. Hayashi, *Phys. Rev. Lett.* **2006**, *96*, 167402.
[12] R. Driben, A. Husakou, J. Herrmann, *Opt. Express* **2009**, *17*, 17989.
[13] M. Samoc, A. Samoc, B. Luther-Davies, Z. Bao, L. Yu, B. Hsieh, U. Scherf, *JOSA B* **1998**, *15*, 817.
[14] M. Sheik-Bahae, A. A. Said, T.-H. Wei, D. J. Hagan, E. W. Van Stryland, *IEEE J. Quantum Electron.* **1990**, *26*, 760.
[15] E. W. Van Stryland, M. Sheik-Bahae, in *Materials Characterization and Optical Probe Techniques: A Critical review*, vol. *10291*, SPIE, Bellingham, Washington **1997**, pp. 488–511.
[16] X. Tian, H.-s. Lu, T. Qian, W. Zhou, J. Yang, X. Yang, S. Ju, Z.-G. Li, Y. Song, *Appl. Phys. Lett.* **2024**, *124*, 15.
[17] S. A. Maier, *Plasmonics: Fundamentals and Applications*, vol. *1*, Springer, Berlin **2007**.
[18] M. Kauranen, A. V. Zayats, *Nat. Photonics* **2012**, *6*, 737.
[19] J. Butet, P.-F. Brevet, O. J. Martin, *ACS Nano* **2015**, *9*, 10545.
[20] A. Bouhelier, M. Beversluis, A. Hartschuh, L. Novotny, *Phys. Rev. Lett.* **2003**, *90*, 013903.
[21] M. Lippitz, M. A. van Dijk, M. Orrit, *Nano Lett.* **2005**, *5*, 799.
[22] G. Li, S. Zhang, T. Zentgraf, *Nat. Rev. Mater.* **2017**, *2*, 5.
[23] O. S. Ojambati, R. Chikkaraddy, W. M. Deacon, J. Huang, D. Wright, J. J. Baumberg, *Nano Lett.* **2020**, *20*, 4653.
[24] M. Wang, T. Wang, O. S. Ojambati, T. J. Duffin, K. Kang, T. Lee, E. Scheer, D. Xiang, C. A. Nijhuis, *Nat. Rev. Chem.* **2022**, *6*, 681.
[25] S. M. Kostritskii, M. Aillerie, E. Kokanyan, in *Fundamentals of Laser-Assisted Micro-and Nanotechnologies 2013*, vol. *9065*, SPIE, Bellingham, Washington **2013**, pp. 67–73.
[26] S. Debrus, J. Lafait, M. May, N. Pinçon, D. Prot, C. Sella, J. Venturini, *J. Appl. Phys.* **2000**, *88*, 4469.
[27] M. Wang, T. Wang, O. S. Ojambati, T. J. Duffin, K. Kang, T. Lee, E. Scheer, D. Xiang, C. A. Nijhuis, *Nat. Rev. Chem.* **2022**, 1.
[28] J. J. Baumberg, J. Aizpurua, M. H. Mikkelsen, D. R. Smith, *Nat. Mater.* **2019**, *18*, 668.
[29] X. Liu, S. Guo, H. Wang, L. Hou, *Opt. Commun.* **2001**, *197*, 431.
[30] R. Ganeev, A. Ryasnyansky, *Phys. Status Solidi A* **2005**, *202*, 120.
[31] Y. Zhu, H. I. Elim, Y.-L. Foo, T. Yu, Y. Liu, W. Ji, J.-Y. Lee, Z. Shen, A. T.-S. Wee, J. T.-L. Thong, C.-H. Sow, *Adv. Mater.* **2006**, *18*, 587.
[32] J. M. Zárate-Reyes, O. Sanchez-Dena, E. Flores-Romero, J. Peralta-Angeles, J. Reyes-Esqueda, J. Cheang-Wong, *Opt. Mater.* **2021**, *111*, 110616.
[33] D. Petrov, *JOSA B* **1996**, *13*, 1491.
[34] R. Ganeev, *Appl. Phys. B* **2008**, *91*, 273.
[35] D. D. Smith, Y. Yoon, R. W. Boyd, J. K. Campbell, L. A. Baker, R. M. Crooks, M. George, *J. Appl. Phys.* **1999**, *86*, 6200.
[36] P. Schmitt, P. Paul, W. Li, Z. Wang, C. David, N. Daryakar, K. Hanemann, N. Felde, A.-S. Munser, M. F. Kling, S. Schröder, A. Tünnermann, A. Szeghalmi, *Coatings* **2023**, *13*, 787.
[37] O. S. Ojambati, K. B. Arnardóttir, B. W. Lovett, J. Keeling, J. J. Baumberg, *Nanophotonics* **2024**, *13*, 2679.
[38] A. Lombardi, A. Demetriadou, L. Weller, P. Andrae, F. Benz, R. Chikkaraddy, J. Aizpurua, J. J. Baumberg, *ACS Photonics* **2016**, *3*, 471.